NeuroImage 147 (2017) 233–242

Contents lists available at ScienceDirect

NeuroImage

journal homepage: www.elsevier.com/locate/neuroimage

Heterogeneous increases of regional cerebral blood flow during preterm brain development: Preliminary assessment with pseudo-continuous arterial spin labeled perfusion MRI

Minhui Ouyang[a,b,c], Peiying Liu[b,d], Tina Jeon[a,b,c], Lina Chalak[e], Roy Heyne[e], Nancy K. Rollins[f], Daniel J. Licht[g], John A. Detre[h,i], Timothy P.L. Roberts[a,i], Hanzhang Lu[b,d], Hao Huang[a,b,i,*]

[a] Radiology Research, Children's Hospital of Philadelphia, PA, United States
[b] Advanced Imaging Research Center, University of Texas Southwestern Medical Center, TX, United States
[c] Biomedical Engineering Joint Graduate Program, University of Texas at Arlington-University of Texas Southwestern Medical Center, TX, United States
[d] Department of Radiology, School of Medicine, Johns Hopkins University, MD, United States
[e] Department of Pediatrics, University of Texas Southwestern Medical Center, Dallas, TX, United States
[f] Departemnt of Radiology, Children's Medical Center, Dallas, TX, United States
[g] Division of Neurology, Children's Hospital of Philadelphia, PA, United States
[h] Department of Neurology, University of Pennsylvania, PA, United States
[i] Department of Radiology, Perelman School of Medicine, University of Pennsylvania, PA, United States

ARTICLE INFO

Keywords:
Preterm brain
Cerebral blood flow
Arterial spin labeled
Heterogeneous
Cortical microstructure
Brain development

ABSTRACT

The human brain develops rapidly during 32-45 postmenstrual weeks (PMW), a critical stage characterized by dramatic increases of metabolic demand. The increasing metabolic demand can be inferred through measurements of regional cerebral blood flow (CBF), which might be coupled to regional metabolism in preterm brains. Arterial spin labeled (ASL) perfusion MRI is one of the few viable approaches for imaging regional CBF of preterm brains, but must be optimized for the extremely slow blood velocity unique in preterm brains. In this study, we explored the spatiotemporal CBF distribution in newborns scanned at the age of 32-45PMW using a pseudo-continuous ASL (pCASL) protocol adapted to slow blood flow in neonates. A total of 89 neonates were recruited. PCASL MRI was acquired from 34 normal newborns and phase contrast (PC) images from 19 newborns. Diffusion tensor images (DTI) were acquired from all 89 neonates for measuring cortical fractional anisotropy (FA), which characterizes cortical microstructure. Reproducible CBF measurements were obtained with the adjusted pCASL sequence. Global CBF measurement based on PC MRI was found to double its value in the 3rd trimester. Regional CBF increases were heterogeneous across the brain with a significantly higher rate of CBF increase in the frontal lobe and a lower rate of CBF increase in the occipital lobe. A significant correlation was found between frontal cortical CBF and cortical FA measurements ($p < 0.01$). Increasing CBF values observed in the frontal lobe corresponded to lower FA values, suggesting that dendritic arborization and synaptic formation might be associated with an elevated local CBF. These results offer a preliminary account of heterogeneous regional CBF increases in a vital early developmental period and may shed the light on underlying metabolic support for cortical microstructural changes during the developmental period of 32-45PMW. Preterm effects and limitations of pCASL techniques in newborns need to be carefully considered for interpretation these results.

1. Introduction

During the 3rd trimester, dramatic cellular and molecular processes, including cell proliferation, migration (Jacobson, 1991; Rabinowicz, 1986), synapse formation, dendritic arborization (Bystron et al., 2008; Huttenlocher and Dabholkar, 1997) and myelination (Yakovlev and Lecours, 1967), take place in the cerebral cortex. Both glucose and oxygen, essential substrates for maintaining cellular and molecular processes during brain development, are delivered through cerebral blood flow (CBF). Rapid brain maturation requires both increases in whole brain CBF and localized increases as brain function begins to differentiate (see Silbereis et al., 2016 for review).

* Corresponding author at: Radiology Research, Children's Hospital of Philadelphia, 34th street and Civic Center blvd, Philadelphia, PA 19104, United States.
E-mail address: huangh6@email.chop.edu (H. Huang).

http://dx.doi.org/10.1016/j.neuroimage.2016.12.034
Received 14 October 2016; Accepted 13 December 2016
Available online 14 December 2016

Quantifying both global and regional CBF thus provide critical information about brain physiology and functional development. Furthermore, cortical microstructural architecture is also dramatically reshaped during 32-45 postmenstrual weeks (PMW) (Bystron et al., 2008; Kostovic and Jovanov-Milosevic, 2006; Rakic, 1972, 1995; Sidman and Rakic, 1973). However, how these regional microstructural changes relate to regional CBF changes has yet to be elucidated.

Arterial spin labeled (ASL) (Detre and Alsop, 1999) perfusion magnetic resonance imaging (MRI) provides a noninvasive approach for quantifying regional CBF without exposure to ionizing radiation or the administration of exogenous contrast agents, and hence is especially suitable for regional CBF measurements of infants and young children. ASL has become a reliable tool to study regional CBF in the brains of infants (e.g. Wang et al., 2008), children (e.g. Jain et al., 2012; Wang et al., 2003), adolescents (e.g. Satterthwaite et al., 2014) and adults (e.g. Chalela et al., 2000). ASL has also been applied to study regional CBF in neonate brains in normal (De Vis et al., 2013; Miranda et al., 2006) and pathological conditions (e.g. congenital heart disease, cardiac arrest or hypoxic-ischemic encephalopathy) (Licht et al., 2004; De Vis et al., 2015, 2014; Massaro et al., 2013; Nagaraj et al., 2015; Pienaar et al., 2012; Varela et al., 2014; Wintermark et al., 2011). In these studies, regional CBF measures in both frontal and occipital cortex were significant higher in healthy neonates at 40-43PMW than those at 30-33PMW (De Vis et al., 2013). In contrast to research on regional CBF in relatively older children or adults, the major challenge unique in neonate brains is the extremely slow blood velocity (Wu et al., 2010). To date, there has been no standardized ASL protocol established for neonate brains, and optimization of ASL perfusion MRI protocol is needed. Moreover, successful measurement of the spatiotemporal dynamics of regional CBF during the critical developmental period of 32-45PMW would provide new insights into metabolic demand of underlying differentiated cellular activities. The associated brain microstructural changes can be inferred by the metric measurements with diffusion tensor imaging (DTI) (Basser et al., 1994). As an alternative to ASL, phase contrast (PC) MRI has been used to quantify global CBF (Bakker et al., 1999) of children and adolescents in a number of studies (e.g. Aslan et al., 2010; Jain et al., 2012). However, PC MRI slice locations have yet to be optimized to adapt to the complex anatomy of arteries at the neck region of neonate brains (Liu et al., 2014).

In this study, we explored the spatiotemporal dynamics of regional CBF during 32-45PMW using pseudo-continuous ASL (pCASL) (Alsop et al., 2015; Dai et al., 2008). We measured global CBF with PC MRI to reveal the extent of global CBF increase during the age of 33-42PMW. Using fractional anisotropy (FA) derived from DTI as a means of quantifying changes in regional cortical microstructure of the preterm brains (McKinstry et al., 2002; Delpolyi et al., 2005; Ball et al., 2013; Yu et al., 2015), we also explored the relationship between regional CBF and cortical microstructure. A pCASL protocol was adjusted to be adapted to the slow cerebral blood velocity seen in the neonates, and pCASL, PC MRI and DTI were acquired from part (for pCASL and PC MRI) and the entire (for DTI) cohort of 89 neonates, respectively. Without additional description, the age defined in postmenstrual week according to Engle's policy statement (Engle et al., 2004) was used.

2. Material and methods

2.1. Neonate subjects

This study was approved by the local Institutional Review Board (IRB) of The University of Texas Southwestern Medical Center. 89 normal neonates were recruited from Parkland Memorial Hospital, Dallas, TX, USA, for research of normal prenatal and perinatal human brain development. These infants were selected through rigorous screening procedures by a board-certified neonatologist (LC). Exclusion criteria included the maternal drug or alcohol abuse during pregnancy; grade III-IV intraventricular hemorrhage; periventricular leukomalacia; hypoxic-ischemic encephalopathy; body or heart malformations; chromosomal abnormalities, lung disease or bronchopulmonary dysplasia; sepsis; necrotizing enterocolitis requiring intestinal resection or complex feeding/nutritional disorders; defects or anomalies of the forebrain, brainstem or cerebellum; brain tissue dysplasia or hypoplasia; abnormal meninges; alterations in the pial or ventricular surface; or white matter lesions. A pediatric radiologist (NR) with 25 years of experience confirmed no structural or signal abnormality with a dulcet image pattern appropriate for postmenstrual age after reading the MRI scans. Written and informed consent was obtained from the parents.

2.2. MRI data acquisition

All MRI scans were performed on the preterm and term-born neonates after their births with a 3T Philips Achieva System. The neonates were fed before the MRI scan and wrapped with a vacuum immobilizer to minimize motion. No sedation was used for all MR data acquisition. All 89 neonates underwent the diffusion MRI and structural MRI. The pCASL and PC MRI sequences were applied to a subcohort of these neonates. As there is no standard neonate pCASL sequence as a reference, both 3D gradient spin-echo (GRASE) and 2D multi-slice echo-planar imaging (EPI) were adjusted from adult human protocol to achieve good image quality and used as the readout component of pCASL sequence. Sequence parameters are described in detail in subsequent sections. A total of 16 neonates underwent ASL with a 3D GRASE pCASL sequence adjusted to be adapted to neonate brains. Of these, 12 datasets (age at scan: 33.3-41.1weeks, 36.6 ± 2.6weeks; age at birth: 27.7-39.3weeks, 31.9 ± 3.1weeks; 7 Male/5 Female) were retained and 4 datasets affected by severe motion were removed. Another 18 neonates underwent ASL with 2D multi-slice pCASL sequence, also adjusted to be adapted to neonate brains. Of these, 10 datasets (age at scan: 32.7-45.1weeks, 37.7 ± 3.8weeks; age at birth: 30.0-41.4weeks, 34.9 ± 3.8weeks; 9 Male/1 Female) were kept for further analysis and 8 datasets affected by severe motion were removed. 19 neonates underwent global CBF quantification with a PC sequence. Of these, 15 datasets (age at scan: 33.9-41.6weeks, 36.4 ± 2.2weeks; age at birth: 27.7-41.3weeks, 32.6 ± 3.9weeks; 8 Male/7 Female) were kept for further analysis and 4 datasets affected by severe motion were removed. The detailed information of all scanned neonates is shown in Table 1.

2.2.1. PC MRI for global CBF measurement

MR images from a representative preterm infant at 35PMW were used to demonstrate the PC MR acquisition (Fig. 1). A time-of-flight angiogram was acquired with axial slices encompassing a slab covering the foramen magnum (see mid-sagittal image on left panel of Fig. 1). The imaging parameters of the angiogram were: TR/TE/flip angle=20ms/3.45ms/18°; field of view (FOV)=100×100 mm^2, in-plane imaging resolution=1×1 mm^2, 20 slices acquired with slice thickness=1 mm, thickness of saturation slab above the imaging slab=60 mm, and the scan duration=19 s. The four feeding arteries, including bilateral internal carotid artery (ICA) and vertebral artery (VA), could be well visualized in the generated angiogram on the right middle panel of Fig. 1. Based on the angiogram, the slices for the PC MRI of ICAs were placed at the level of the foramen magnum and the slices for the PC MRI of VAs were placed between the two turns in V3 segments (at approximately the level of the C1 vertebral column), shown in the right panel of Fig. 1. Image parameters of PC MRI were: FOV=120×120 mm^2, in-plane imaging resolution=0.5×0.5 mm^2, single slice with a thickness of 3 mm, maximum velocity encoding=10 cm/s, non-gated, 4 repetitions, and scan duration of each artery=24 s. As shown in Fig. 1, the cross-section of the target artery with higher intensity can be appreciated in each PC image.

Table 1
Information of the neonates with acceptable pCASL or PC MRI scans.

Index of neonates	Age at birth (PMW)	Age at scan (PMW)	Preterm /full-term birth	Weight at birth (g)	Weight at scan (g)	Gender (M/F)	Mode of delivery (C/V)*	Feeding practice (B/F)#	Antibiotic exposure during pregnancy	Estimated blood T1 (ms)	Estimated Hematocrit	3D GRASE ASL	Multi-slice ASL	PC MRI	Auxiliary scan for M_b^0
1	30.0	33.7	PT	1550	1920	M	V	B	Yes	1681	0.500	–	√	–	–
2	34.1	35.9	PT	1835	1945	M	V	B	Yes	1664	0.510	–	√	√	–
3	34.0	36.1	PT	2486	2545	M	V	B	Yes	1664	0.510	–	√	√	–
4	38.0	38.1	FT	3180	2910	M	V	B	Yes	1632	0.530	–	√	–	–
5	40.6	40.7	FT	3950	3920	M	V	B	Yes	1617	0.540	–	√	–	–
6	31.1	32.7	PT	1490	1420	M	C	B	Yes	1681	0.500	–	√	–	–
7	34.0	37.6	PT	1710	2105	F	V	B	Yes	1656	0.515	–	√	–	–
8	32.4	45.3	PT	2210	2600	M	C	B	Yes	1557	0.580	–	√	–	–
9	41.4	41.6	FT	3885	3790	M	V	B	Yes	1624	0.535	–	√	–	–
10	33.9	35.6	PT	2130	2262	M	V	B	Yes	1664	0.510	–	√	–	–
11	31.0	33.3	PT	1330	1500	F	V	B	Yes	1681	0.500	√	–	–	–
12	33.0	33.9	PT	2115	2055	M	C	B	Yes	1681	0.500	√	–	√	√
13	33.6	35.0	PT	2090	2230	M	C	B	Yes	1672	0.505	√	–	√	–
14	33.1	35.1	PT	2280	2625	M	C	B	Yes	1672	0.505	√	–	–	–
15	28.4	36.1	PT	900	2280	M	V	B	Yes	1664	0.510	√	–	–	–
16	31.0	36.3	PT	850	2110	F	C	B	Yes	1664	0.510	√	–	√	–
17	31.0	37.3	PT	1330	1500	F	C	B	Yes	1648	0.520	√	–	–	–
18	27.7	37.4	PT	1070	2390	F	V	B	Yes	1648	0.520	√	–	√	√
19	34.4	39.9	PT	1940	3010	M	V	B	Yes	1617	0.540	√	–	–	√
20	39.3	40.3	FT	3350	3035	M	V	B	Yes	1617	0.540	√	–	–	–
21	28.7	41.1	PT	1360	3270	M	V	B	Yes	1617	0.540	√	–	–	–
22	31.9	34.6	PT	1450	1890	F	C	B	Yes	1681	0.500	√	–	√	√
23	28.9	34.9	PT	1500	2960	M	V	B	Yes	–	–	–	–	√	–
24	29.7	34.7	PT	1240	2012	F	C	B	Yes	–	–	–	–	√	–
25	29.7	36.4	PT	1240	2350	F	C	B	Yes	–	–	–	–	√	–
26	30.0	34.7	PT	1330	1821	F	C	B	Yes	–	–	–	–	√	–
27	34.7	36.3	PT	1715	1884	M	V	B	Yes	–	–	–	–	√	–
28	29.7	37.1	PT	1085	1530	M	C	B	Yes	–	–	–	–	√	–
29	40.7	40.7	FT	3680	3680	M	C	B	Yes	–	–	–	–	√	–
30	41.3	41.6	FT	2960	2710	F	V	B	Yes	–	–	–	–	√	–

*: C/V: C for C-section and V for Vaginal birth. #: B/F: B for breast feeding and F for formula. PT/FT: preterm / full-term. -: data not available. √: data available.

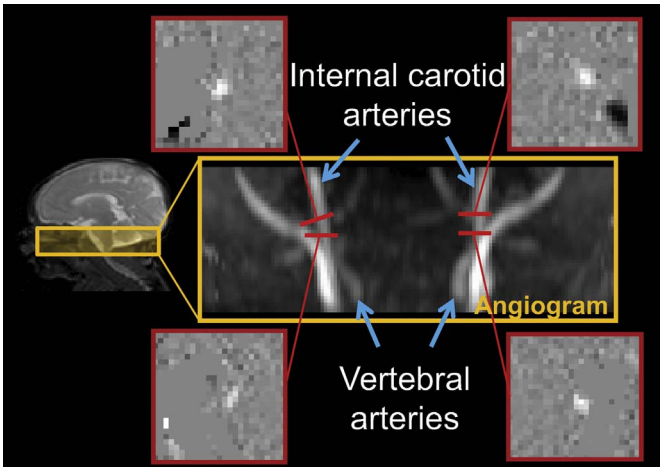

Fig. 1. Phase-contrast (PC) MRI for global cerebral blood flow (CBF) measurement. The coronal view of the angiogram in the right middle panel shows the feeding arterials, namely internal carotid and vertebral arteries, with anatomical location of the 3D angiography delineated in a T2 weighted sagittal image on the left panel. The four slices of the PC MRI scans were positioned perpendicular to the respective feeding arteries on the angiogram, shown as red bars. The four phase images of the target arteries from the PC MRI scans are shown on the four panels surrounding the angiogram.

2.2.2. 3D GRASE pCASL and 2D multi-slice pCASL for regional CBF measurement

PCASL labeling (Dai et al., 2008) combined with either 3D GRASE or multi-slice EPI as readout component was used to measure regional CBF. In the first several neonates (data not included in the Results due to non-optimized results before finalized adjustment), the position of labeling slab and post labeling delay (PLD) time were tested on multiple possible values to adapt to slow blood flow velocity of the neonates. The middle of labeling slab was placed between the bottom of the pons and the bottom of the cerebellum as an optimized position of labeling slab (Fig. 2a). The bottom of the pons was selected as the optimized labeling location, based on clearer gray-white matter contrast and fewer artifacts in the CBF map (shown in the panel of Fig. 2a with green contour). These adjusted protocols were thereby used in the rest of the study. PLD durations of 1525 ms, 1900 ms, 2000 ms, 2300 ms and 2500 ms were tested in a few neonates (see supplemental information for CBF maps with different PLDs). Extremely slow blood velocity in newborn brain and subsequently longer time for labeled blood to perfuse into the brain tissue in the imaging slab require a longer PLD. Since the ASL signal undergoes T1 decay after labeling, the trade-off of using a longer PLD time is a decrease of the signal and noise ratio (SNR) in labeled images. As shown in the panel with green contour in Fig. 2b, the longest PLD duration of 2500ms, yielded less artifacts and optimal gray-white matter contrast in the CBF map, was selected for the rest of the study. In addition, two global inversion background suppression (BS) pulses were added between labeling and readout component in the 3D GRASE pCASL sequence to suppress the static tissue signal (gray/white matter) and increase the SNR of ASL signal (Ye et al., 2002). After T_1 relaxation simulation of gray/white matter and control/ labeled blood, we found that it is optimal to put BS1 at 2350 ms and BS2 at 3734 ms in the pulse sequence with most gray/white matter tissue signal intensity suppressed (Fig. 2c). The voxel size of 3D GRASE and Multi-slice pCASL are 3.5×3.5×4 mm^3 and 3.5×3.5×3.5 mm^3, respectively. The finalized imaging parameters of 3D GRASE pCASL and 2D multi-slice pCASL sequences for neonate brains are listed in Table 2.

2.2.3. DTI

DTI was acquired on all 89 neonates with a single-shot, EPI sequence with Sensitivity Encoding parallel imaging scheme (SENSE,

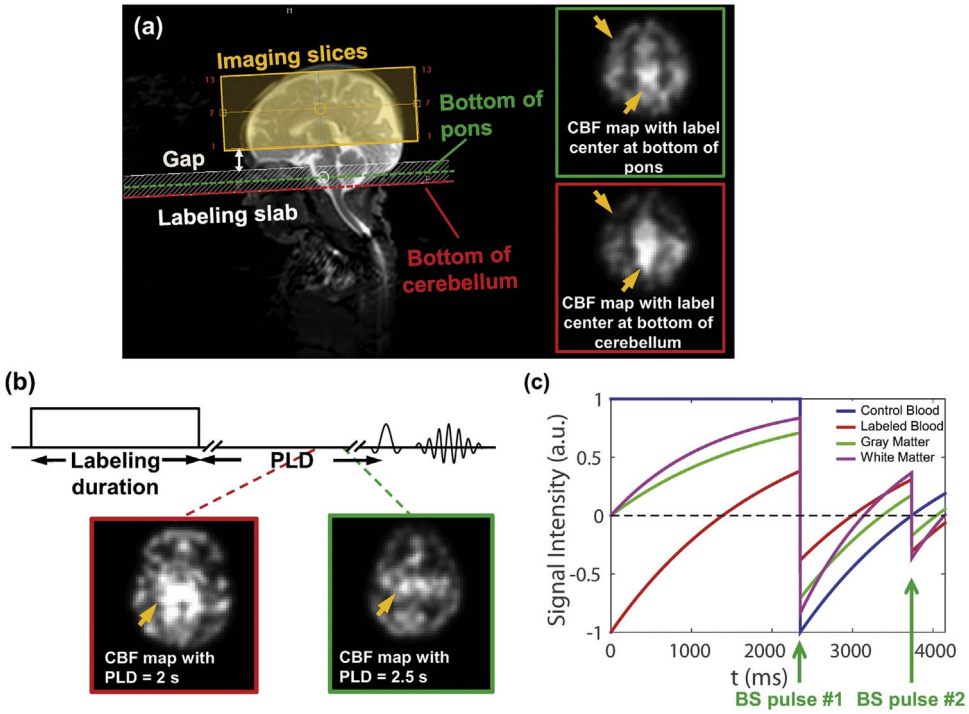

Fig. 2. Adjustments of major pCASL sequence parameters for preterm brains. (a) Selection of positioning of labeling slab for 3D GRASE and 2D multi-slice pCASL: Imaging slices (yellow shaded box) and labeling slab (white shaded box) were positioned to be parallel to the anterior commissure-posterior commissure (AC-PC) line. The middle of labeling slab was chosen to be located at the bottom of the pons (green dashed line) instead of bottom of cerebellum (red dashed line) in preterm brain. (b) Selection of post labeling delay (PLD) time for 3D GRASE and 2D multi-slice pCASL: PLD was chosen to be 2.5 s instead of 2 s. The yellow arrows in CBF maps (a, b) point to the regions with less artifacts using the optimized sequence (highlighted with green contour). (c) Optimization of the timing of background suppression (BS) pulses for 3D GRASE pCASL using T1 relaxation simulation. Optimal sequence parameters for 3D GRASE and 2D multi-slice pCASL are listed in Table 2. Of the note, the two CBF maps in (b) were from two different subjects.

Table 2
After sequence adjustment to be adapted to preterm brains, finalized imaging parameters for the 3D GRASE and multi-slice pCASL are listed below.

Parameter	3D GRASE pCASL	Multi-slice pCASL
Scan mode	3D	MS
Fast imaging mode	GRASE	EPI
Field of view (mm^2)	140×140	160×160
Matrix	40×40	46×46
Number of slice	13	16
Acquisition resolution (mm^3)	3.5×3.5×4	3.5×3.5×3.5
TR/TE (msec)	4462/18	4380/7.4
Label duration (msec)	1650	1650
Post label delay (msec)	2500	2500
Label slab thickness (mm)	16	16
Label offset (mm)	42	36
Background suppression time 1 (msec)	2350	–
Background suppression time 2 (msec)	3734	–
Middle of labeling slab location	bottom of Pons	bottom of Pons
Dynamic scan	30	40
SENSE factor	2	2.5
Scan time	~5 min	~6 min

reduction factor=2). The DTI imaging in-plane resolution was 1.5×1.5 mm^2 with a FOV of 168×168 mm^2. Axial slices of 1.6 mm thickness without gap were acquired parallel to the anterior-posterior commissure (AC-PC) line. A total of 60 slices covered the entire brain. The diffusion weighting was encoded with 30 independent directions (Jones et al., 1999) and the b-value was 1000 s/mm^2.

2.2.4. T2-weighted image

T2-weighted image was acquired on all 87 neonates with following parameters: turbo spin echo sequence, TR/TE=3000/135 ms, 65 slices, voxel size=1.5×1.5×1.6 mm^3, FOV=160×160×104 mm^3. T2-weighted images have superior gray and white matter contrast for neonate brains and were used for anatomical guidance and brain volume calculation.

2.3. MRI postprocessing

2.3.1. Global CBF measurement

PC MRI provides a quantitative measurement of the blood flow velocity, v, in the ICAs and VAs. The blood velocity can be converted to flow rate by integrating over the cross-section of the vessels with equation

$$F = \int vdA \tag{1}$$

where F is blood flow with the unit ml/sec and A is the cross-sectional area of the blood vessel with the unit mm^2. The brain volume was measured from the T2-weighted image as parenchyma volume (gray matter+white matter volume). The global CBF was calculated with the equation:

$$\text{global CBF} = F/(\rho * \text{brainvolume}) \tag{2}$$

The brain tissue density ρ was assumed as 1.06 g/mL in Eq. (2) (Dittmer, 1961; Herscovitch and Raichle, 1985).

2.3.2. Regional CBF measurement

In ASL MRI, CBF can be derived from the difference between "label" images in which arterial blood has been magnetically-labeled and "control" image in which the arterial blood has not been labeled. Specifically, regional CBF value can be estimated from pCASL data using the basic model described in ASL white paper (Alsop et al., 2015):

$$f_{pCASL}(x, y, z) = \frac{6000*\lambda.\ \Delta M(x, y, z)*e^{\frac{PLD(z)}{T_{1a}}}}{2\alpha.\ M_b^0.\ T_{1a}.\left(1 - e^{\frac{-LabelDur}{T_{1a}}}\right)}\ [ml/100g/min] \tag{3}$$

where $f_{pCASL}(x, y, z)$ is the blood flow at voxel (x,y,z) obtained from pCASL in milliliters of blood per minute per 100 g brain tissue. $\Delta M(x, y, z)$ is the difference between dynamic-averaged signal intensity in control image and that in the label image at voxel (x, y, z). Here α, the labeling efficiency, is 0.92 according to the relationship of labeling efficiency and blood velocity in the previous study (Aslan et al., 2010) with the blood velocity of 10.77 ± 4.44 cm/sec measured from PC MRI of 14 neonates; λ, the blood-brain partition coefficient, is 0.9 mL/g (Herscovitch and Raichle, 1985); *PLD(z)*, the post labeling delay time at the slice *z*, is 2500 ms for images acquired with 3D GRASE pCASL sequence and 2500+(*z*-1)*w for images acquired with multi-slice pCASL sequence, where w=35 ms is the slice timing delay between adjacent slices; *LabelDur*, the labeling duration, is 1650ms; T_{1a}, T_1 of arterial blood, was obtained for each subject based on blood T1-hematocrit curve (Liu et al., 2015). The subject-specific hematocrit was estimated with the subjects' age at scan based on the hematocrit-age curve (Jopling et al., 2009). The estimated $T_{1\alpha}$ and hematocrit of each neonate scanned with pCASL are listed in Table 1. To scale the signal intensities of the subtracted ASL images to absolute CBF units, the value of equilibrium magnetization of brain tissue (M_b^0) is needed. This value was obtained with Eq. (4.1) for 3D GRASE pCASL and Eq.(4.2) for multi-slice pCASL:

$$M_b^0 = M_{thalamus\_slice} / \left((1 - 2\bullet e^{\frac{-(PLD+LabelDur-BS2)}{T_{1tissue}}} + 2\bullet e^{\frac{-(PLD+LableDur-BS1)}{T_{1tissue}}} - e^{\frac{-(PLD+LableDur)}{T_{1tissue}}}\right) \tag{4.1}$$

$$M_b^0 = M_{thalamus\_slice} / \left(1 - e^{\frac{-TR}{T_{1tissue}}}\right) \tag{4.2}$$

where $T_{1tissue}$, the T_1 of brain tissue, is 2500 ms (Conklin et al., 2008; Lu et al., 2004; Williams et al., 2005); the timings of two BS pulses, *BS1* and *BS2*, are 2350 ms and 3734 ms, respectively; $M_{thalamus\_slice}$ is the average signal intensity in the ROI including entire brain on a slice containing thalamus in the control image. To improve the accuracy of regional CBF estimation from 3D GRASE pCASL scan, either a short auxiliary scan (to correct for M_b^0 estimation) or PC MRI can be acquired to scale the absolute CBF calculated from Eq. (3). The estimation of M_b^0 from an auxiliary scan using identical readout module as 3D GRASE pCASL but without labeling or background suppression components was more accurate than the estimation of M_b^0 directly from the main3D GRASE pCASLscanusing Eq. (4.1) (Alsop et al., 2015). PC MRI could not be used to normalize the regional CBF because the 3D pCASL scan did not cover the whole brain in this study. Instead, an auxiliary scan was performed to estimate $M_{bauxscan}^0$ using Eq. (4.2). 4 neonates underwent this auxiliary scan successfully, while other infants' auxiliary scans were either not useful due to severe motion or not conducted due to limited scan time. An averaged scaling factor was obtained with these 4 neonates' auxiliary scans to correct for all CBF maps from 3D GRASE pCASL acquisition (see "Correction of absolute CBF from 3D ASL scan" in Supplemental information for more details).

2.3.3. Measurement of frontal and occipital CBF with ROI

ROIs were drawn manually in the frontal and occipital cortical regions in both hemispheres of the CBF maps. They were drawn in the same axial slice at consistent anatomical location across subjects. Each ROI included 10 contiguous cortical voxels in each hemisphere. As an example, delineation of the frontal and occipital ROI on CBF maps of a 34.6PMW and a 37.4PMW brain are displayed in Fig. 3. Averaged CBF in frontal or occipital ROIs were calculated from ROIs drawn on both hemispheres for each subject.

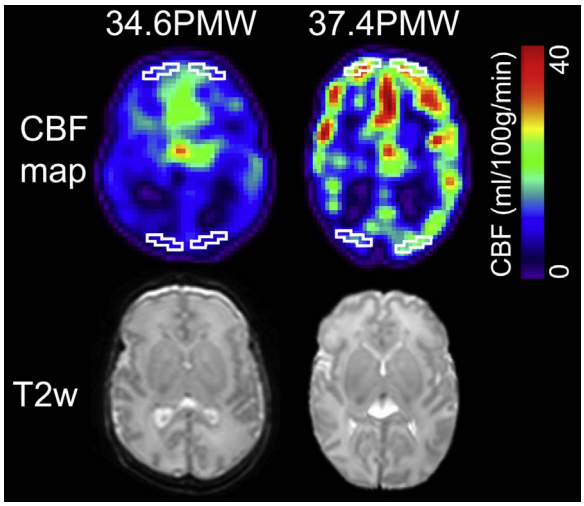

Fig. 3. Heterogeneous frontal and occipital CBF with regions of interest (ROIs), contoured with white lines, were placed in frontal and occipital areas. Axial CBF maps from a representative preterm brain with younger age (34.6PMW) and a preterm brain with older age (37.4PMW) are displayed in color on left and right panel of the figure, respectively, with color bar encoding the CBF values. Corresponding T2 weighted images are displayed in the bottom for anatomical guidance.

2.3.4. Measurement of cortical skeletonized FA with DTI

Automated image registration (AIR) (Woods et al., 1998) was applied to raw diffusion weighted images to correct distortion caused by eddy current. The standard tensor fitting was conducted with DTIStudio (Jiang et al., 2006) to generate the FA map. To minimize partial volume effects, cortical skeletonized FA values (Yu et al., 2015) were used to explore the relationship between regional CBF and FA in the cortex. Cortical skeletons were obtained with the skeletonization function of TBSS in FSL ⟨http://fsl.fmrib.ox.ac.uk/fsl/fslwiki/TBSS⟩ based on averaged cortical FA maps for preterm brains at 33 and 36PMW or averaged gray matter segmentation maps for neonate brains at 39PMW (Yu et al., 2015). Cortical skeleton of individual neonate brain was obtained by inverse registration from averaged templates at 33, 36 or 39PMW. The template having the PMW closest to the PMW of the individual neonate brain was used for inverse registration. Note that high FA was observed not only at the WM but also cortical plate for preterm brain FA at 33 and 36PMW (Yu et al., 2015).

2.4. Statistical analysis

2.4.1. Reproducibility analysis

3 randomly chosen subjects were scanned twice with separate but identical finalized 3D GRASE pCASL sequence in the same session for reproducibility analysis. Intraclass correlation coefficient (ICC) (Jain et al., 2012; Shrout and Fleiss, 1979) was calculated to assess the reproducibility of CBF maps obtained from two repetitions of ASL scans.

2.4.2. Correlation between the global CBF and age

Linear regression between the global CBF measurement and the postmenstrual age at the scan time was performed to evaluate the age dependent global CBF changes during 33–42PMW. To remove the effects of postnatal age (i.e. the chronological age defined in Engle et al., 2004), partial correlation between global CBF and postmenstrual age was conducted with the postnatal age added as a regressor using R software.

2.4.3. Paired t-test between frontal and occipital CBF

To test if the CBF distribution is heterogeneous among different brain regions, paired t-test between CBF measurements averaged from

frontal ROI voxels and those averaged from occipital ROI voxels was conducted. The frontal and occipital CBF measurements were paired according to the individual subject.

2.4.4. Correlation between frontal or occipital CBF and age

Linear regression was conducted between mean CBF in frontal or occipital ROI from both 3D GRASE and 2D multi-slice pCASL acquisitions and the postmenstrual age at the time of scan. To consider the postnatal age effects, postnatal age was added as a regressor in the correlation between CBF and the scan age. In addition, comparison between the slopes of age-dependent linear trend lines of frontal CBF and occipital CBF was conducted with a mixed-effects model as follows:

$$CBF_i=\mu+\beta_1*I_i+\beta_2*age_i+\beta_3*(I\bullet age)_i+\epsilon_i \quad (5)$$

where CBF_i was CBF frontal or occipital CBF measurement from the *ith* participated neonates; μ was the overall mean of CBF measurement, I_i was the indicator variable with I_i=1 for frontal CBF measurement and I_i=0 for occipital CBF measurement; age_irepresented the age of *ith* neonate; $(I\bullet age)_i$ was the age-region interaction term and ϵ_i was the error term; β_1, β_2 and $\beta_3$represented the parameters to be estimated for I_i, age_i and $(I\bullet age)_i$, respectively. The statistical procedures were performed using R software ⟨https://www.r-project.org/⟩.

2.4.5. Correlation between cortical CBF and cortical skeletonized FA measurement

Linear regression between averaged regional CBF and averaged cortical skeletonized FA values in the same frontal ROIs as those shown in Fig. 3 was conducted. Since both CBF-age and FA-age (e.g. Huang et al., 2013; Yu et al., 2015) correlations could be significant, it is possible the correlation between CBF and FA is due to age. To remove the age effect, partial correlation between cortical FA and cortical CBF in the frontal ROIs was conducted using R software.

3. Results

3.1. Age-dependent increase of global CBF for neonates

Fig. 4 shows the age-dependent increase of global CBF derived from PC MRI of 14 infants aged 33 to 42PMW. Global CBF increases significantly (r=0.65, p=0.01) with postmenstrual age. Specifically, the global CBF increases from 8.4 ml/100 g/min at 33PMW to 21.6 ml/100 g/min at 42PMW with an increase rate of 1.22 ml/100 g/min per PMW. Note that the value of global CBF at 42PWM almost doubles the value of global CBF at 33PMW. After removing the effects of postnatal age, global CBF still shows significant age-dependent increase (r=0.62, p=0.02).

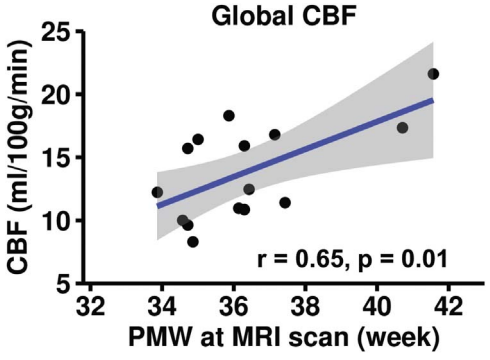

Fig. 4. Global CBF measurements from PC MRI increase significantly ($p < 0.01$) and dramatically with age in preterm brains of 33–42PMW. Each black circle represents global CBF measurement from a preterm infant. Fitted confidence intervals are shown as the shaded area.

3.2. Heterogeneous regional CBF distributions in the individual neonate brains

Paired t-test shows that CBF measurements at frontal regions (28.2 ± 8.3 ml/100 g/min) are significantly higher ($p < 0.001$) than those at occipital regions (19.6 ± 5.7 ml/100 g/min) for newborn brains during 32-45PMW. This heterogeneity can also be appreciated in CBF maps of two randomly selected preterm brains at 34.6PMW and 37.4PMW shown in Fig. 3.

3.3. Heterogeneous regional CBF increase during 32-45PMW

Age-dependent frontal and occipital CBF trend lines are shown in Fig. 5a and Fig. 5b, respectively. Both frontal and occipital CBF values increase significantly with age (r=0.79 and $p < 0.001$ for frontal CBF; and r=0.52, $p < 0.05$ for occipital CBF). In addition, a significantly faster CBF increase (p=0.027) can be appreciated at the frontal regions with the increase rate of 2.08 ml/100 g/min per PMW (Fig. 5a), which is 1.14 ml/100 g/min per PMW larger than and approximately double of the CBF increase rate of 0.94 ml/100 g/min per PMW at the occipital regions (Fig. 5b). The increase rates were obtained based on fitted linear trend lines of frontal and occipital CBF during 32-45PMW. After regression of postnatal age, significantly age-dependent increases of regional CBF were still found in both frontal (r=0.75 and p=0.001) and occipital cortex (r=0.56 and p=0.008). The CBF measurements from two datasets were combined in Fig. 5 to increase statistical power, after confirming there was no significant difference in regional CBF (frontal or occipital) increase rate measured by background-suppressed 3D GRASE pCASL versus multi-slice pCASL (see Supplemental information).

3.4. Relationship between cortical CBF and cortical FA in the frontal region

A significant negative correlation (r=-0.62, $p < 0.01$) was observed between cortical CBF and cortical FA in frontal regions of neonates aged 32-45PMW, as demonstrated in Fig. 6a. After removing the age effect, significant negative partial correlation (r=−0.44, $p < 0.05$) was still obtained between cortical CBF and cortical FA in frontal regions. Higher regional CBF is associated with lower cortical FA at the frontal region. Representative cortical FA and CBF maps acquired at 37.4PMW are shown in Figs. 6b and 6c, respectively. As indicated in Fig. 6b, FA values extracted from a cortical skeleton were used to minimize partial volume effects for cortical FA measurements.

3.5. Reproducibility of the CBF measurement

Fig. 7 shows CBF maps from two repetitions of pCASL scans of 3 randomly chosen preterm infants. The ‘rep1’ and ‘rep2’ present the CBF maps of each preterm infant consecutively scanned with the same pCASL sequence in one session. The ICC values for three preterm infants were 0.75, 0.85 and 0.91 respectively, indicating moderate-to-strong reproducibility (ICC from 0.75 to 0.95).

4. Discussion

Heterogeneous increases of regional cortical CBF were demonstrated using pCASL data of neonate brains in the age range of 32-45PMW. Frontal CBF increases faster than occipital CBF (Fig. 5). In parallel to regionally heterogeneous CBF increases, global CBF increases were also demonstrated using PC MRI during this period. Specifically, the measured global CBF value at 42PMW almost doubles the global CBF value at 33PMW (Fig. 4), suggesting dramatic increase of whole brain metabolic needs during the 3rd trimester. A strong negative correlation between the frontal CBF and frontal cortical FA measurements (Fig. 6) was also found. Imaging parameters of pCASL

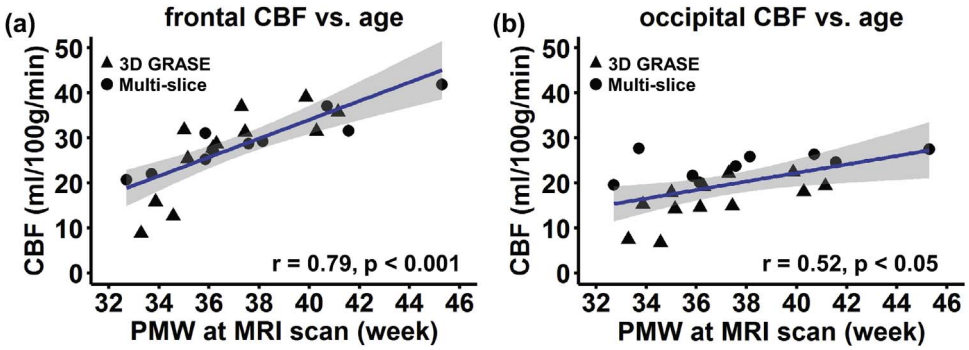

Fig. 5. Regionally heterogeneous increases of CBF measurements in developing preterm brains revealed by combined datasets from 3D GRASE and 2D multi-slice pCASL acquisitions. Regional CBF measurements increase significantly with age in both frontal (a) and occipital (b) cortex. Relatively higher frontal CBF increase rate can be appreciated. Each data point (black triangle or black circle) in (a, b) represents regional CBF of one preterm infant, with black triangle and black circle indicating regional CBF measurement with 3D GRASE pCASL and multi-slice pCASL, respectively. Fitted confidence intervals are shown as the shaded area.

sequences were selected to adapt to extremely slow blood velocity of the neonate brains and these sequences had achieved moderate-to-strong reproducibility for regional CBF measurements (Fig. 7). Relatively comprehensive scan ages of neonate brains ranged from 32 to 45PMW, covering majority of the 3rd trimester. Significant age-dependent increases of both global and regional CBF (after removing the postnatal age effects) during this critical developmental period were revealed for both understanding early brain development and meeting the need for health care of preterm infants.

4.1. Significant global CBF increases during preterm brain development

Dramatic and rapid brain development takes place in the 3rd trimester. In such a short period, the cerebral cortex volume increases 4-fold (Huppi et al., 1998; Limperopoulos et al., 2005). Inside the cerebral cortex, cellular and molecular processes including dendritic arborization, synaptic formation, and cell differentiation (Innocenti and Price, 2005; Marín-Padilla, 1992; Rakic, 1988; Sidman and Rakic, 1982) reshape the brain configuration. The scan age of neonate brains in this study, namely 33–42PMW, covers the majority of the 3rd trimester. Despite the difference of intrauterine and extrauterine brain growth (discussed in details in "4.4 Considerations and future perspectives" section below), the observed CBF measurements obtained from neonate brains over 33-42PMW might reflect increase of cerebral energy consumption (du Plessis, 2009) associated with cellular processes in the cortical development.

Global CBF measurements obtained around 33-42PMW have previously been reported using various imaging modalities. Global CBF in preterm neonates (mean age at 40PMW) was reported to be 4.9 to 23 ml/100 g/min (Altman et al., 1988) using positron emission tomography (PET). With near infrared spectroscopy (NIRS), global CBF was found to range from 7 to 33 ml/100 g/min in neonates aged 26–44PMW (Edwards et al., 1988). Another NIRS study showed that global CBF ranged from 6.3 to 15.2 ml/100 g/min in very preterm infants aged 24 to 31PMW (Meek et al., 1998). Using xenon clearance, global CBF was reported to be 4.3–18.9 ml/100 g/min in preterm infants less than 33PMW (Greisen and Trojaborg, 1987). Global CBF values obtained in the present study using PC MRI ranged from 8.4 to

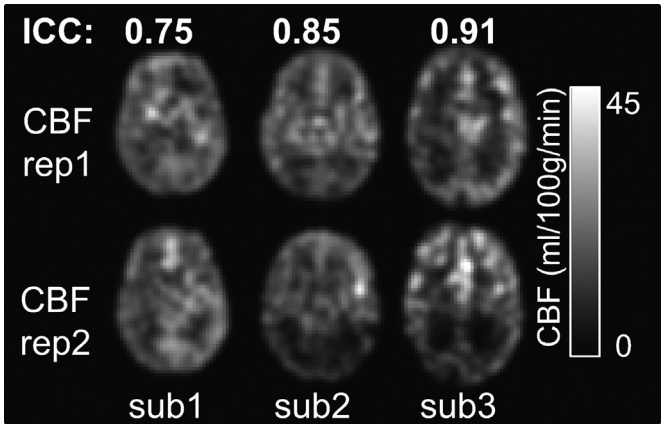

Fig. 7. Test-retest reliability of the measured CBF maps from three randomly selected preterm infants with optimized 3D GRASE pCASL sequence. Same slices of CBF maps from two repetitions of scans are shown as 'rep1' and 'rep2'. The calculated intraclass correlation coefficients (ICC) are shown on the top of CBF maps. Color bar encodes the CBF values.

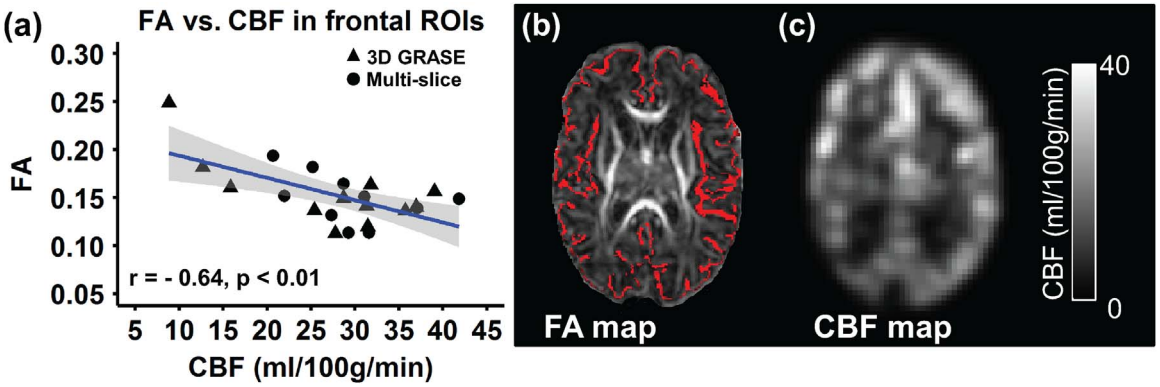

Fig. 6. Correlation between cortical fractional anisotropy (FA) and CBF in the same corresponding frontal region. (a) Regional CBF is significantly ($p < 0.01$) correlated with cortical FA; (b) FA map with cortical skeleton shown in red from a representative preterm infant at 37.4PMW; (c) corresponding CBF map from the same preterm infant. Each data point in (a) represents cortical FA and CBF measurement from one neonate, with black triangle and black circle indicating regional CBF measurement with 3D GRASE pCASL and multi-slice pCASL, respectively. Fitted confidence intervals are shown as the shaded area.

21.6 ml/100 g/min during 33–42PMW (Fig. 4), and are consistent with the previous findings.

4.2. Heterogeneous regional CBF distributions and increases in preterm brains

Although global CBF increases from 32-45PMW, CBF changes are also regionally heterogeneous, with significantly different CBF increase rates in frontal and occipital cortices (Fig. 5). Accordingly, higher frontal CBF increase rates enlarged CBF differences between frontal and occipital regions. Regional differences in CBF during development have also been reported using modalities other than MRI. Using xenon clearance, occipital CBFs have been found significantly lower than frontal and parietal CBF in preterm infants with less than 34 gestational weeks and scanned between 0–240 hours after birth (Baenziger et al., 1995). Similar results were reported in preterm infants aged 26–34PMW with blood flow significantly higher in mesial frontal cortex than that in mesial occipital cortex using single photon emission computed tomography (SPECT) (Borch and Greisen, 1998). Regional heterogeneity in the rates of metabolic maturation for different cerebral cortical regions have also been observed in infants. The PET studies revealed different age-dependent curves of glucose utilization among different brain regions, including primary visual cortex (in occipital cortical region) and middle frontal gyrus, in infants of 0 to 18 months (Chugani and Phelps, 1986). That all neonates were scanned during their natural sleep with their eyes closed and no visual stimuli may also contribute to the consistently low CBF at occipital cortex.

Compared to regional CBF estimates from pCASL, the global CBF from PC MRI is considered as a more robust CBF measurement. PC MRI yields blood velocity measurements in the major feeder and therefor provides global CBF even for low flow velocities (Liu et al., 2014; Jain et al., 2014; Varela et al., 2011). PC MRI has been well validated by ultrasound and used for quantitative flow measurements for more than 2 decades (Evans et al., 1993). On the other hand, PC MRI offers for the entire brain only a single global CBF value which is averaged CBF in the whole brain tissue. Hence, global CBF is much less informative compared to regional CBF measurements (one CBF value per brain voxel) offered by pCASL.

With whole brain cortical FA mapping, inhomogeneous regional microstructural changes reflected by cortical FA were found in mid-fetal (Huang et al., 2013) and late-fetal (Ball et al., 2013; Yu et al., 2015) human brain development. Heterogeneity of CBF distribution and increases were also observed in Fig. 3 and Fig. 5, respectively. By correlating frontal cortical FA (quantifying cortical microstructure) to corresponding frontal CBF (inferring metabolic need) across the age of 32-45PMW, Fig. 6 demonstrated that higher CBF is associated with lower FA. The exact underlying mechanism is not known. Further investigation with larger sample size on the relationship of histology-FA and metabolic rate-CBF is warranted for understanding the mechanism of the observed association in Fig. 6.

4.3. Considerations and future perspectives

This study is limited by several factors including preterm effects, pCASL techniques and small sample size. The study may serve as a proof-of-concept that the pCASL technique has the potential to understand age-dependent regional CBF changes in early neurodevelopment. Due to relatively small sample size of neonate subjects undergoing scan with 3D GRASE pCASL or 2D multi-slice pCASL, we combined datasets acquired with both protocols to study age-dependent regional CBF changes. To integrate two datasets, we corrected absolute CBF measurement from 3D GRASE pCASL by multiplying a scaling factor. Unlike 2D multi-slice pCASL, the 3D GRASE pCASL is known to be affected by inaccurate estimation of M_b^0 from its control image (Alsop et al., 2015). To address this issue, we conducted auxiliary scans and obtained a scaling factor to correct for absolute CBF measurement from 3D GRASE pCASL. In addition, we carefully confirmed no significant differences between regional CBF increase rate from 3D GRASE pCASL dataset only and regional CBF increase rate from multi-slice pCASL dataset only. However, the absolute values of occipital CBF from 3D pCASL are significantly lower compared to those from multi-slice pCASL, while no significant differences were found for absolute values of frontal CBF between 3D and multi-slice pCASL. The lower occipital CBF associated to 3D pCASL might be related to global inversion background suppression, which could invert spins of a neonate heart. With the body coil length of the scanner 60 cm, head coil length 30 cm and the neonate head centered in the head coil and body coil, the body coil will inevitably invert the arterial spins pumped from the heart of a neonate at or close to the boundary of the body coil. However, the inversion at or close to the boundary of the body coil is generally weak, much less than 180 or even 90 degrees (e.g. Schepers et al., 2005). It might be the case that with the bolus arrival time to occipital lobe longer than frontal lobe (e.g. MacIntosh et al., 2010), higher fraction of incoming spins to the occipital lobe were affected by global inversion, resulting in lower CBF in occipital lobe with 3D pCASL. The detailed statistical models and analysis comparing CBF measurements from these two pCASL protocols can be found in Supplemental information. Based on these analyses, 3D pCASL with slab selective inversion pulse for background suppression is recommended for neonates, consistent to the recommended ASL applied for general subjects in white paper (Alsop et al., 2015). Future studies with CBF measurements of neonate brains from uniform pCASL protocol are warranted to validate the findings in the present study. The moderate-to-strong reproducibility in Fig. 7 may be related to the procedure that two tests were conducted within one-session. But regional CBF changes from day to day in neonates. To remove the effects of CBF changes due to rapid brain development between two dates, we conducted reproducible tests within one scan session instead of two scan sessions on different dates. Exposure to the extrauterine environment could affect the measured CBF distribution and dynamics, but these effects would be relatively subtle compared with the dramatic developmental factor during the 3rd trimester (Bourgeois et al., 1989; Kostovic, 1990). After regressing the postnatal age, we found the correlation between frontal or occipital CBF and age was still significant. Of the note, it is likely that the regional CBF deviation from the normal CBF developmental curve due to preterm effects could become apparent in years subsequent to premature birth. As shown in Table 1, a small portion of term-born neonates (2 out of 15 for global CBF and 4 out of 22 for regional CBF) were included. The inclusions of term-born neonates could make the CBF trend lines in Fig. 4 and Fig. 5 to deviate from those of the preterm brains only due to known differences between preterm brains at term-equivalent age and term-born brains (e.g. Ball et al., 2013; Akazawa et al., 2016). The factor of inclusion of term-born neonates cannot be tested effectively with small sample size in this study. The deviations might not significantly alter the age-dependent CBF change patterns given the small portion of included term-born neonates. Future studies with larger sample size of both preterm and term-born neonates are needed to understand the CBF differences between preterm brains at term-equivalent age and term-born brains. Several major imaging parameters of pCASL were adjusted to be adapted to neonate brains. To better estimate the regional CBF from ASL, future studies will benefit from collecting subject-specific information for tuning these imaging parameters. For example, individual subject's hematocrit can be used for subject-specific blood T1 estimation (Liu et al., 2015). In addition, larger sample size may reveal nonlinear regional CBF change curves instead of simple linear lines used in this study, and longitudinal dataset may remove the effects caused by the individual differences.

5. Conclusion

In summary, the present study revealed spatiotemporally heterogeneous increases of cortical regional CBF in preterm brains scanned

with pCASL MRI during 32-45PMW, a period of rapid brain development. Dramatic global CBF increases were found with PC MRI in parallel with heterogeneous regional CBF increases based on pCASL MRI. In addition, significant correlations between cortical CBF and cortical FA measurements in the frontal cortex suggest an association between active cellular processes causing microstructural changes and local CBF increases meeting the metabolic demand of these processes. Multimodal MRI provides a noninvasive means for characterizing changes in cortical structure and function during preterm brain development. Relatively high reproducibility of CBF measurements obtained in present study demonstrate the potential of using pCASL to study the regional CBF of neonate brains aged 32-45PMW on a 3T MRI scanner.

Funding and disclosure

This study was supported by NIH (Grant nos. R01 MH092535, U54 HD086984, P41 EB015893, R01 MH084021, and R21 NS085634). The authors report no biomedical financial interests or potential conflicts of interest.

Acknowledgements

The authors are grateful to Neonatal-Perinatal Division in University of Texas at Southwestern Medical Center and MRI technologists in Radiology Department from Children's Medical Center of Dallas for their support and assistance, and also the parents of the scanned neonates for their essential involvement in this study.

Appendix A. Supplementary material

Supplementary data associated with this article can be found in the online version at http://dx.doi.org/10.1016/j.neuroimage.2016.12.034.

References

Akazawa, K., Chang, L., Yamakawa, R., Hayama, S., Buchthal, S., Alicata, D., Andres, T., Castillo, D., Oishi, K., Skranes, J., Ernst, T., Oishi, K., 2016. Probabilistic maps of the white matter tracts with known associated functions on the neonateal brain atlas: application to evaluate longitudinal developmental trajectories in term-born and preterm-born infants. Neuroimage 128, 167–179.

Alsop, D.C., Detre, J.A., Golay, X., Günther, M., Hendrikse, J., Hernandez-Garcia, L., Lu, H., MacIntosh, B.J., Parkes, L.M., Smits, M., 2015. Recommended implementation of arterial spin-labeled perfusion MRI for clinical applications: a consensus of the ISMRM perfusion study group and the European consortium for ASL in dementia. Magn. Reson. Med. 73, 102–116.

Altman, D.I., Powers, W.J., Perlman, J.M., Herscovitch, P., Volpe, S.L., Volpe, J.J., 1988. Cerebral blood flow requirement for brain viability in newborn infants is lower than in adults. Ann. Neurol. 24, 218–226.

Aslan, S., Xu, F., Wang, P.L., Uh, J., Yezhuvath, U.S., van Osch, M., Lu, H., 2010. Estimation of labeling efficiency in pseudocontinuous arterial spin labeling. Magn. Reson. Med. 63, 765–771.

Baenziger, O., Jaggi, J.L., Mueller, A.C., Morales, C.G., Lipp, A.E., Duc, G., Bucher, H.U., 1995. Regional differences of cerebral blood flow in the preterm infant. Eur. J. Pediatr. 154, 919–924.

Bakker, C.J., Hoogeveen, R.M., Viergever, M.A., 1999. Construction of a protocol for measuring blood flow by two-dimensional phase-contrast MRA. J Magn. Reson. Imaging 9, 119–127.

Ball, G., Srinivasan, L., Aljabar, P., Counsell, S.J., Durighel, G., Hajnal, J.V., Rutherford, M.A., Edwards, A.D., 2013. Development of cortical microstructure in the preterm human brain. Proc. Natl. Acad. Sci. U.S.A. 110, 9541–9546.

Basser, P.J., Mattiello, J., LeBihan, D., 1994. MR diffusion tensor spectroscopy and imaging. Biophys. J. 66, 259–267.

Borch, K., Greisen, G., 1998. Blood flow distribution in the normal human preterm brain. Pediatr. Res. 43, 28–33.

Bourgeois, J.P., Jastreboff, P.J., Rakic, P., 1989. Synaptogenesis in visual cortex of normal and preterm monkeys: evidence for intrinsic regulation of synaptic overproduction. Proc. Natl. Acad. Sci. U.S.A. 86, 4297–4301.

Bystron, I., Blakemore, C., Rakic, P., 2008. Development of the human cerebral cortex: boulder committee revisited. Nat. Rev. Neurosci. 9, 110–122.

Chalela, J.A., Alsop, D.C., Gonzalez-Atavales, J.B., Maldjian, J.A., Kasner, S.E., Detre, J.A., 2000. Magnetic resonance perfusion imaging in acute ischemic stroke using continuous arterial spin labeling. Stroke 31, 680–687.

Chugani, H.T., Phelps, M.E., 1986. Maturational changes in cerebral function in infants determined by 18FDG positron emission tomography. Science 231, 840–843.

Conklin, J., Winter, J.D., Thompson, R.T., Gelman, N., 2008. High-contrast 3D neonate brain imaging with combined T1-and T2-weighted MPRAGE. Magn. Reson. Med. 59 (5), 1190–1196.

Dai, W., Garcia, D., de Bazelaire, C., Alsop, D.C., 2008. Continuous flow-driven inversion for arterial spin labeling using pulsed radio frequency and gradient fields. Magn. Reson. Med. 60, 1488–1497.

De Vis, J.B., Petersen, E.T., de Vries, L.S., Groenendaal, F., Kersbergen, K.J., Alderliesten, T., Hendrikse, J., Benders, M.J., 2013. Regional changes in brain perfusion during brain maturation measured non-invasively with Arterial Spin Labeling MRI in neonates. Eur. J. Radiol. 82, 538–543.

De Vis, J.B., Petersen, E.T., Alderliesten, T., Groenendaal, F., de Vries, L.S., van Bel, F., Benders, M.J., Hendrikse, J., 2014. Non-invasive MRI measurements of venous oxygenation, oxygen extraction fraction and oxygen consumption in neonates. Neuroimage 95, 185–192.

De Vis, J.B., Hendrikse, J., Petersen, E.T., de Vries, L.S., van Bel, F., Alderliesten, T., Negro, S., Groenendaal, F., Benders, M.J., 2015. Arterial spin-labelling perfusion MRI and outcome in neonates with hypoxic-ischemic encephalopathy. Eur. Radiol. 25, 113–121.

delpolyi, A.R., Mukherjee, P., Gill, K., Henry, R.G., Partridge, S.C., Veeraraghavan, S., Jin, H., Lu, Y., Miller, S.P., Ferriero, D.M., Vigneron, D.B., Barkovich, A.J., 2005. Comparing microstructural and macrostructural development of the cerebral cortex in premature newborns: diffusion tensor imaging versus cortical gyration. Neuroimage 27 (3), 579–586.

Detre, J.A., Alsop, D.C., 1999. Perfusion magnetic resonance imaging with continuous arterial spin labeling: methods and clinical applications in the central nervous system. Eur. J. Radiol. 30, 115–124.

Dittmer, D.S., 1961. Blood and Other Body Fluids 15. Federation of American Societies for Experimental Biology, Washington, DC, 326–327.

Edwards, A.D., Wyatt, J.S., Richardson, C., Delpy, D.T., Cope, M., Reynolds, E.O., 1988. Cotside measurement of cerebral blood flow in ill newborn infants by near infrared spectroscopy. Lancet 2, 770–771.

Engle, W.A., American Academy of Pediatrics Committee on Fetus and Newborn, 2004. Age terminology during the perintal period. Pediatrics, vol. 114, pp.1362–1364.

Evans, A.J., Iwai, F., Grist, T.A., Sostman, H.D., Hedlund, L.W., Spritzer, C.E., Negro-Vilar, R.O.S.A., Beam, C.A., Pelc, N.J., 1993. Magnetic resonance imaging of blood flow with a phase subtraction technique: in vitro and in vivo validation. Investig. Radiol. 28 (2), 109–115.

Greisen, G., Trojaborg, W., 1987. Cerebral blood flow, PaCO2 changes, and visual evoked potentials in mechanically ventilated, preterm infants. Acta Paediatr. 76, 394–400.

Herscovitch, P., Raichle, M.E., 1985. What is the correct value for the brain-blood partition coefficient for water. J. Cereb. Blood Flow Metab. 5, 65–69.

Huang, H., Jeon, T., Sedmak, G., Pletikos, M., Vasung, L., Xu, X., Yarowsky, P., Richards, L.J., Kostovic, I., Sestan, N., Mori, S., 2013. Coupling diffusion imaging with histological and gene expression analysis to examine the dynamics of cortical areas across the fetal period of human brain development. Cereb. Cortex 23, 2620–2631.

Huppi, P.S., Warfield, S., Kikinis, R., Barnes, P.D., Zientara, G.P., Jolesz, F.A., Tsuji, M.K., Volpe, J.J., 1998. Quantitative magnetic resonance imaging of brain development in premature and mature newborns. Ann. Neurol. 43, 224–235.

Huttenlocher, P.R., Dabholkar, A.S., 1997. Regional differences in synaptogenesis in human cerebral cortex. J. Comp. Neurol. 387, 167–178.

Innocenti, G.M., Price, D.J., 2005. Exuberance in the development of cortical networks. Nat. Rev. Neurosci. 6, 955–965.

Jacobson, M., 1991. Developmental Neurobiology. Plenum Press, New York.

Jain, V., Duda, J., Avants, B., Giannetta, M., Xie, S.X., Roberts, T., Detre, J.A., Hurt, H., Wehrli, F.W., Wang, D.J., 2012. Longitudinal reproducibility and accuracy of pseudo-continuous arterial spin-labeled perfusion MR imaging in typically developing children. Radiology 263, 527–536.

Jiang, H., van Zijl, P.C., Kim, J., Pearlson, G.D., Mori, S., 2006. DtiStudio: resource program for diffusion tensor computation and fiber bundle tracking. Comput. Methods Prog. Biomed. 81, 106–116.

Jones, D.K., Horsfield, M.A., Simmons, A., 1999. Optimal strategies for measuring diffusion in anisotropic systems by magnetic resonance imaging. Magn. Reson. Med. 42, 515–525.

Jopling, J., Henry, E., Wiedmeier, S.E., Christensen, R.D., 2009. Reference ranges for hematocrit and blood hemoglobin concentration during the neonatal period: data from a multihospital health care system. Pediatrics 123 (2), e333–e337.

Kostovic, I., 1990. Structural and histochemical reorganization of the human prefrontal cortex during perinatal and postnatal life. Prog. Brain Res. 85 (223-239), 239–240.

Kostovic, I., Jovanov-Milosevic, N., 2006. The development of cerebral connections during the first 20-45 weeks' gestation. Semin. Fetal Neonatal Med. 11, 415–422.

Licht, D.J., Wang, J., Silvestre, D.W., Nicolson, S.C., Montenegro, L.M., Wernovsky, G., Tabbutt, S., Durning, S.M., Shera, D.M., Gaynor, J.W., Spray, T.L., Clancy, R.R., Zimmerman, R.A., Detre, J.A., 2004. Preoperative cerebral blood flow is deminished in neonates with severe congnital heart defects. J. Thorac. Cardiovasc. Surg. 128 (6), 841–849.

Limperopoulos, C., Soul, J.S., Gauvreau, K., Huppi, P.S., Warfield, S.K., Bassan, H., Robertson, R.L., Volpe, J.J., du Plessis, A.J., 2005. Late gestation cerebellar growth is rapid and impeded by premature birth. Pediatrics 115, 688–695.

Liu, P., Huang, H., Rollins, N., Chalak, L.F., Jeon, T., Halovanic, C., Lu, H., 2014. Quantitative assessment of global cerebral metabolic rate of oxygen (CMRO2) in neonates using MRI. NMR Biomed. 27, 332–340.

Liu, P., Chalak, L.F., Krishnamurthy, L.C., Mir, I., Peng, Sl, Huang, H., Lu, H., 2015. T1 and T2 values of human neonatal blood at 3 T: dependence on hematocrit, oxygenation, and temperature. Magn. Reson. Med. 75, 1730–1735.

Lu, H., Clingman, C., Golay, X., van Zijl, P.C., 2004. Determining the longitudinal relaxation time (T1) of blood at 3.0 T. Magn. Reson. Med. 52, 679–682.
MacIntosh, B.J., Filippini, N., Chappell, M.A., Woolrich, M.W., Mackay, C.E., Jezzard, P., 2010. Assessment of arterial arrival times derived from multiple inversion time pulsed arterial spin labeling MRI. Magn. Reson. Med. 63, 641–647.
Marín-Padilla, M., 1992. Ontogenesis of the pyramidal cell of the mammalian neocortex and developmental cytoarchitectonics: a unifying theory. J. Comp. Neurol. 321, 223–240.
Massaro, A.N., Bouyssi-Kobar, M., Chang, T., Vezina, L.G., du Plessis, A.J., Limperopoulos, C., 2013. Brain perfusion in encephalopathic newborns after therapeutic hypothermia. AJNR Am. J. Neuroradiol. 34, 1649–1655.
McKinstry, R.C., Mathur, A., Miller, J.H., Ozcan, A., Snyder, A.Z., Schefft, G.L., Almli, C.R., Shimony, J.S., Shiran, S.I., Neil, J.J., 2002. Radial organization of developing preterm human cerebral cortex revealed by non-invasive water diffusion anisotropy MRI. Cereb. Cortex 12, 1237–1243.
Meek, J.H., Tyszczuk, L., Elwell, C.E., Wyatt, J.S., 1998. Cerebral blood flow increases over the first three days of life in extremely preterm neonates. Arch. Dis. Child Fetal Neonatal Ed. 78, F33–F37.
Miranda, M.J., Olofsson, K., Sidaros, K., 2006. Noninvasive measurements of regional cerebral perfusion in preterm and term neonates by magnetic resonance arterial spin labeling. Pediatr. Res. 60, 359–363.
Nagaraj, U.D., Evangelou, I.E., Donofrio, M.T., Vezina, L.G., McCarter, R., du Plessis, A.J., Limperopoulos, C., 2015. Impaired global and regional cerebral perfusion in newborns with complex congenital heart disease. J. Pediatr. 167, 1018–1024.
Pienaar, R., Paldino, M.J., Madan, N., Krishnamoorthy, K.S., Alsop, D.C., Dehaes, M., Grant, P.E., 2012. A quantitative method for correlating observations of decreased apparent diffusion coefficient with elevated cerebral blood perfusion in newborns presenting cerebral ischemic insults. Neuroimage 63, 1510–1518.
du Plessis, A.J., 2009. Cerebral blood flow and metabolism in the developing fetus. Clin. Perinatol. 36, 531–548.
Rabinowicz, T., 1986. The differentiated maturation of the cerebral cortex. In: Falkner, F., Tanner, J.M. (Eds.), Human Growth 2. Plenum, New York, 385–410.
Rakic, P., 1972. Mode of cell migration to the superficial layers of fetal monkey neocortex. J. Comp. Neurol. 145, 61–83.
Rakic, P., 1988. Specification of cerebral cortical areas. Science 241, 170–176.
Rakic, P., 1995. Radial versus tangential migration of neuronal clones in the developing cerebral cortex. Proc. Natl. Acad. Sci. U.S.A. 92, 11323–11327.
Satterthwaite, T.D., Shinohara, R.T., Wolf, D.H., Hopson, R.D., Elliott, M.A., Vandekar, S.N., Ruparel, K., Calkins, M.E., Roalf, D.R., Gennatas, E.D., Jackson, C., Erus, G., Prabhakaran, K., Davatzikos, C., Detre, J.A., Hakonarson, H., Gur, R.C., Gur, R.E., 2014. Impact of puberty on the evolution of cerebral perfusion during adolescence. Proc. Natl. Acad. Sci. U.S.A. 111, 8643–8648.
Schepers, J., van Osch, M.J.P., Bartels, L.W., Heukels, S.N., Viergever, M.A., Nicolay, K., 2005. The effects of B_1 field inhomogeneity and the nonselective inversion profile on the kinetics of FAIR-based perfusion MRI. Mag. Reson. Med. 53, 1355–1362.
Shrout, P.E., Fleiss, J.L., 1979. Intraclass correlations: uses in assessing rater reliability. Psychol. Bull. 86, 420–428.
Sidman, R.L., Rakic, P., 1973. Neuronal migration, with special reference to developing human brain: a review. Brain Res. 62, 1–35.
Sidman, R.L., Rakic, P., 1982. Development of the human central nervous system. Histology and Histopathology of the Nervous System. IL, Springfield. p. 3–145.
Silbereis, J.C., Pochareddy, S., Zhu, Y., Li, M., Sestan, N., 2016. The cellular and molecular landscapes of the developing human central nervous system. Neuron 89, 248–268.
Varela, M., Petersen, E.T., Golay, X., Hajnal, J.V., 2014. Cerebral blood flow measurements in infants using look–locker arterial spin labeling. J. Magn. Reson. Imaging. 41, 1591–1600.
Varela, M., Hajnal, J.V., Petersen, E.T., Golay, X., Merchant, N., Larkman, D.J., 2011. A method for rapid in vivo measurement of blood T1. NMR Biomed. 24, 80–88.
Wang, J., Licht, D.J., Jahng, G.H., Liu, C.S., Rubin, J.T., Haselgrove, J., Zimmerman, R.A., Detre, J.A., 2003. Pediatric perfusion imaging using pulsed arterial spin labeling. J. Magn. Reson. Imaging. 18, 404–413.
Wang, Z., Fernández-Seara, M., Alsop, D.C., Liu, W.-C., Flax, J.F., Benasich, A.A., Detre, J.A., 2008. Assessment of functional development in normal infant brain using arterial spin labeled perfusion MRI. Neuroimage 39, 973–978.
Williams, L.A., Gelman, N., Picot, P.A., Lee, D.S., Ewing, J.R., Han, V.K., Thompson, R.T., 2005. Neonatal brain: regional variability of in vivo MR imaging relaxation rates at 3.0 T– initial experimence. Radiology 235 (2), 595–603.
Wintermark, P., Hansen, A., Gregas, M.C., Soul, J., Labrecque, M., Robertson, R.L., Warfield, S.K., 2011. Brain perfusion in asphyxiated newborns treated with therapeutic hypothermia. AJNR Am. J. Neuroradiol. 32, 2023–2029.
Woods, R.P., Grafton, S.T., Holmes, C.J., Cherry, S.R., Mazziotta, J.C., 1998. Automated image registration: i. General methods and intrasubject, intramodality validation. J. Comput. Assist. Tomogr. 22, 139–152.
Wu, W.C., St Lawrence, K.S., Licht, D.J., Wang, D.J., 2010. Quantification issues in arterial spin labeling perfusion magnetic regionance imaging. Top. Magn. Reson. Imaging. 21 (2), 65–73.
Yakovlev, P.I., Lecours, A.R., 1967. The myelogenetic cycles of regional maturation of the brain. In: Minkowski, A. (Ed.), Regional Development of the Brain in Early Life. Blackwell Science, Oxford, 3–70.
Ye, F.Q., Frank, J.A., Weinberger, D.R., McLaughlin, A.C., 2000. Noise reduction in 3D perfusion imaging by attenuating the static signal in arterial spin tagging (ASSIST). Magn. Reson. Med. 44 (1), 92–100.
Yu, Q., Ouyang, A., Chalak, L., Jeon, T., Chia, J., Mishra, V., Sivarajan, M., Jackson, G., Rollins, N., Liu, S., Huang, H., 2016. Structural development of human fetal and preterm brain cortical plate based on population-averaged templates. Cereb. Cortex 26, 4381–4391, (bhv2).